Thin Solid Films 562 (2014) 195–199

Contents lists available at ScienceDirect

Thin Solid Films

journal homepage: www.elsevier.com/locate/tsf

Electronic and structural characterisation of Cu_3BiS_3 thin films for the absorber layer of sustainable photovoltaics

M.V. Yakushev [a,b,*], P. Maiello [c], T. Raadik [e], M.J. Shaw [a], P.R. Edwards [a], J. Krustok [e], A.V. Mudryi [a,d], I. Forbes [c], R.W. Martin [a]

[a] Department of Physics, SUPA, University of Strathclyde, Glasgow G4 0NG, UK
[b] URFU and Ural Branch of RAS, 620002 Ekaterinburg, Russia
[c] Northumbria Photovoltaics Applications Centre, Northumbria University, Ellison Building, Newcastle upon Tyne NE1 8ST, UK
[d] Scientific-Practical Material Research Centre of the National Academy of Science of Belarus, P. Brovki 19, 220072 Minsk, Belarus
[e] Tallinn University Technology, Ehitajate tee 5, Tallinn 19086, Estonia

ARTICLE INFO

Article history:
Received 1 November 2013
Received in revised form 10 April 2014
Accepted 11 April 2014
Available online 26 April 2014

Keywords:
Thin films
Solar cells
Semiconductors
Electronic structure
Raman spectroscopy
Photoreflectance
Photoluminescence

ABSTRACT

Thin films of *p*-type Cu_3BiS_3 with an orthorhombic wittichenite structure, a semiconductor with high potential for thin film solar cell absorber layers, were synthesised by thermal annealing of Cu and Bi precursors, magnetron sputtered on Mo/glass substrate, with a layer of thermo-evaporated S. The elemental composition, structural and electronic properties are studied. The Raman spectrum shows four modes with the dominant peak at 292 cm^{-1}. Photoreflectance spectra demonstrate two band gaps E_{gX} and E_{gY}, associated with the X and Y valence sub-bands, and their evolution with temperature. Fitting the temperature dependencies of the band-gaps gives values of 1.24 and 1.53 eV for E_{gX} and E_{gY} at 0 K as well as the average phonon energy. Photoluminescence spectra at 5 K reveal two bright and broad emission bands at 0.84 and 0.99 eV, which quench with an activation energy of 40 meV. The photocurrent excitation measurements demonstrate a photoresponse and suggest a direct allowed nature of the band gap.

1. Introduction

Large scale fabrication of thin film solar cells requires the development of photovoltaic (PV) technologies based on cheap and non-toxic elements abundant in the Earth's crust. The current leaders for single junction thin film solar cells [1], namely $Cu(InGa)Se_2$ and CdTe-based devices, have shown major successes but their large scale manufacture faces difficulties due to the limited availability of indium (In) and gallium (Ga) as well as of selenium (Se) and tellurium (Te) [2], and also due to toxicity issues with Se, Cd and Te. There is therefore a high demand for semiconductor compounds for solar cell absorber layers containing low cost, non-toxic, and easy to mine elements with high world reserves. A prime candidate for this is $Cu_2ZnSn(SSe)_4$, which is a further development of $CuInSe_2$ where rare and expensive In/Ga are substituted with cheap and abundant Zn and Sn, alternating in the lattice on the indium site of the chalcopyrite structure [3,4]. However the complexity of this compound could be too challenging due to a very narrow single phase region in its phase diagram resulting in a variety of secondary phases present in the material [3].

Alternative ternary semiconductors based on Cu, S and Bi, a non-toxic element with an estimated reserve exceeding those of In and Ga by two orders of magnitude [5], are potential candidates. One of the leading among these is the natural mineral wittichenite Cu_3BiS_3 with an orthorhombic crystal structure and direct band gap [6,7]. This compound also has a high absorption coefficient of ~10^5 cm^{-1} and can be *p*-type doped [8,9].

However the basic electronic properties vital for development of Cu_3BiS_3 photovoltaic devices are almost unexplored, as reflected in the wide scatter of reported experimentally determined bandgap values from 1.14 [7] to 1.41 eV [8]. Theoretical studies of this compound suggested an indirect band gap of 1.69 eV while the smallest direct band gap was estimated to be of 1.79 eV [10]. A study on defect states and surface passivation of *p*-type Cu_3BiS_3 has recently been reported [11]. Theoretical studies suggest that doping Cu_3BiS_3 with oxygen can be used for the formation of an intermediate band (IB) extending theoretical limit of conversion efficiency for Cu_3BiS_3-based IB solar cell to 46% [12]. There are no publications on experimental studies of the electronic band structure. Neither photoluminescence (PL) nor Raman spectra have been reported.

The most common technique for bandgap measurement is optical absorption. However, multinary compounds can often have deep potential fluctuations [13] generating tails in the absorption spectra [14]

* Corresponding author at: Department of Physics, SUPA, University of Strathclyde, Glasgow G4 0NG, UK.
E-mail address: michael.yakushev@strath.ac.uk (M.V. Yakushev).

http://dx.doi.org/10.1016/j.tsf.2014.04.057

making such analysis difficult. Therefore the bandgap energy calculated from the absorption spectrum could often be incorrect. More reliable techniques for measuring the bandgap are electro- or photoreflectance modulation methods [15].

In this paper we report the fabrication of photosensitive thin films of Cu_3BiS_3 by thermal annealing of metal precursors with a layer of thermo-evaporated S and detailed characterisation of their structural, optical and electronic properties.

2. Experimental details

Thin films of Cu_3BiS_3 were fabricated using a two stage process. At first 0.3 μm thick precursor layers of Cu and Bi were magnetron sputtered on Mo-coated soda-lime glass from 5 N-purity elemental targets. 1.5 μm thick films of 4 N-purity sulphur were thermally evaporated on these precursor layers. Then such structures were heated for 30 min at a temperature of 250 °C in Ar atmosphere at a pressure of 100 Pa. An excess of sulphur was provided in order to ensure full sulphurisation of the precursor layer during the heating process. Hot probe measurements revealed *p*-type conductivity of the synthesised Cu_3BiS_3 material. More information on the synthesis of sulphide compound films by chalcogenisation of magnetron deposited multilayer metallic precursors with a layer of sulphur can be found in references [16–19].

The morphology of the deposited films was analysed using a low-vacuum FEI Quanta FEG 250 environmental scanning electron microscope (SEM) at an electron beam energy of 30 keV. The elemental composition and lateral homogeneity were studied by Cameca SX100 wavelength-dispersive X-ray (WDX) microanalysis at an electron beam energy of 5 keV. The structural properties and the presence of secondary phases were examined by Raman spectroscopy and X-ray diffraction. X-ray diffraction (XRD) measurements were performed using a Bruker D5005 diffractometer (Bragg–Brentano geometry) with Cu Kα1 radiation (λ1/41.5406 Å) at 40 kV and 40 mA and a graphite monochromator.

Photoresponse was measured by immersing the films in a glass cell with 0.2 M aqueous solution of $Eu(NO_3)_3$, as electron scavenging redox electrolyte, using a three electrode configuration with Ag/AgCl reference electrode, counter platinum electrode as well as the molybdenum back contact. Samples were illuminated with 75 Hz chopped monochromated light from a tungsten halogen lamp. The measured photo-current was maximised by adjusting the potential with respect to the reference electrode. Photo-current excitation spectra were recorded using a standard Bentham lock-in amplifier and then normalised against calibrated silicon and germanium photodiodes. Such normalised spectra correspond to the apparent quantum efficiency (AQE).

The photoreflectance (PR) measurements were carried out at temperatures from 10 to 300 K using a 40 cm focal length single grating monochromator, Si detector and closed-cycle helium cryostat. Monochromated light from a halogen lamp was employed as the primary beam whereas the 85 Hz modulated 405 nm line of an 80 mW solid state laser was used as the secondary, pumping beam source. The photoluminescence (PL) measurements were carried out using a 1 m focal length single grating monochromator and the 514 nm line of a 200 mW Ar^+ laser for excitation and either a closed-cycle helium cryostat for temperature resolved measurements or a liquid helium cryostat to analyse excitation intensity dependencies. The PL signal was detected by either an InGaAs photomultiplier tube (PMT) or a photodiode for measurements in the spectral ranges from 0.9 to 1.7 μm and 0.9 to 1.9 μm, respectively.

3. Results and discussion

The cross-section and surface views of the film, shown in Fig. 1(a) and (b), respectively, demonstrate a dense homogeneous layer with an average thickness of 0.7 μm. The cross-section in Fig. 1(a) demonstrates that the film structure is columnar with the column diameter of 0.1 μm.

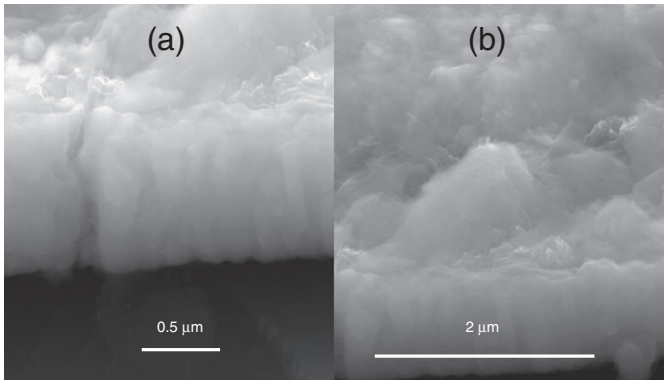

Fig. 1. Cross sectional (a) and surface (b) SEM micrograph views of the Cu_3BiS_3 films.

WDX analysis of the film indicates an elemental composition of 42.4 at.% Cu, 14.7 at.% Bi and 42.9 at.% S with a statistical uncertainty of ±0.6 at.%. This gives a formula of $Cu_{3.00}Bi_{1.04}S_{3.03}$ with uncertainties of ±0.04. A beam energy of 5 keV corresponds to a sampling depth of approximately 0.1 μm. A WDX line-scan across several millimetres of the surface demonstrates good lateral homogeneity of the films, as shown in Fig. 2.

The XRD pattern of the film along with the standard (pdf: 043-1479) orthorhombic pattern shown in Fig. 3 reveals the formation of a wittichenite lattice structure (with the lattice parameters a = 0.7661 nm, b = 1.0388 nm, c = 0.6712 nm), peaks associated with metallic molybdenum and bismuth implying the presence of Bi clusters.

Raman spectra, measured at different points of the films at room temperature, consistently reveal four modes at 96, 125, 264 and 292 cm^{-1} as shown in Fig. 4. The dominant peak at 292 cm^{-1} has a full width at half maximum (FWHM) of 12 cm^{-1}.

The electronic structure of Cu_3BiS_3 was analysed using PR. A modulation of the built-in electric field, created by the surface band bending due to the photo-injection of electron–hole pairs by a chopped incident laser beam, generates differential changes of the complex dielectric function and the amplitude of the PR signal $\Delta R/R$ [15]. Fig. 5 shows room temperature PR spectra, which demonstrate a strong resonance at 1.2 eV.

Decreasing the temperature down to 80 K shifts this resonance towards higher energies and reveals a second resonance at 1.5 eV. Further decrease of temperature, down to 10 K, shifts the resonances further towards higher energies and makes both resonances sharper as

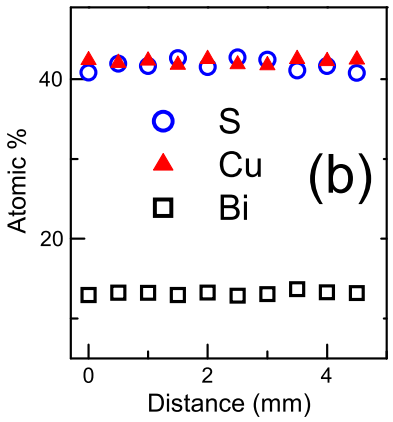

Fig. 2. WDX line-scan of the S, Bi and Cu elemental composition.

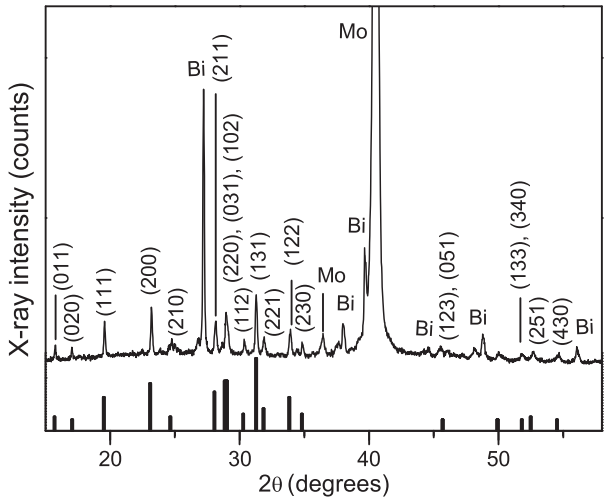

Fig. 3. XRD pattern of Cu_3BiS_3 on Mo coated glass in comparison with standard wittichenite orthorhombic pattern.

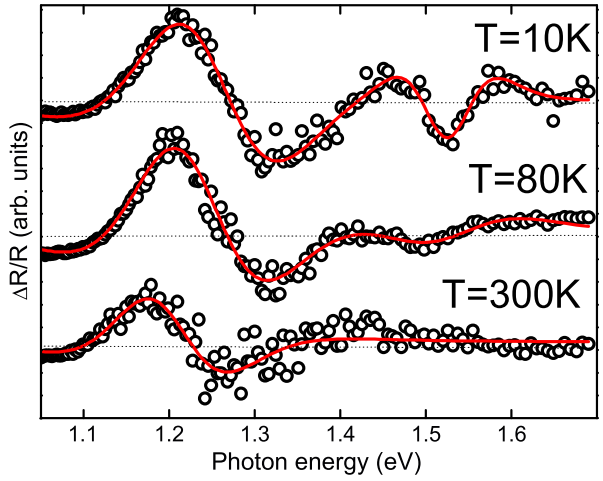

Fig. 5. PR spectra of Cu_3BiS_3 films at different temperatures (b); symbols are experimental PR spectra, and the curves are best fits using Eq. (1). Temperature dependence of the X and Y bandgap energies (c); symbols are experimental E_g, and the curves are best fits using Eq. (2).

shown in Fig. 5. The experimental PR spectra were fitted with the function [20,21],

$$\Delta R/R = \mathrm{Re}\left[\sum_{j=1}^{p} C_j e^{i\theta_j}\left(E - E_{g,j} + i\Gamma_j\right)^{-m}\right] \quad (1)$$

where E is photon energy, C_j, θ_j, $E_{g,j}$ and Γ_j are the amplitude, phase, transition energy and broadening parameter of each resonance, respectively, p is the number of resonances and i is the imaginary unit. A two resonance ($p = 2$) fit was used for low temperature PR spectra. The m parameter is defined by the type of the critical point and $m = 5/2$, corresponding to interband transitions and a three-dimensional critical point, has been assumed for the calculations. The fitted curves for the temperature 10, 80 and 300 K are shown by solid lines in Fig. 5.

Values for E_g for different temperatures, determined using the best fits, are shown in Fig. 6. The presence of two band gaps can be associated with splitting of the valence band. Such splitting has been reported for ternary I–III–IV_2 semiconductor compounds with chalcopyrite structure [22,23]. Measurements on $AgInS_2$, a semiconductor compound which crystallises in two different phases chalcopyrite and orthorhombic, reveal a splitting of the valence band into three sub-bands for both of them [24]. In the chalcopyrite phase the splitting into A, B and C sub-bands occurs due to the simultaneous influence of the crystal field and spin orbit interaction whereas in the orthorhombic one a splitting into X, Y and Z sub-bands is considered to be solely due to the influence of the crystal field. For the orthorhombic structure of Cu_3BiS_3 we use the notations X and Y for the top two bands.

The temperature dependencies of E_{gX} and E_{gY} were fitted with the expression introduced by O'Donnell and Chen [25],

$$E_g(T) = E_g(0) - S\langle\hbar\omega\rangle / [\coth(\langle\hbar\omega\rangle/2kT) - 1] \quad (2)$$

where $E_g(0)$ is the bandgap energy at 0 K, S is a dimensionless coupling constant and $\langle\hbar\omega\rangle$ represents an average phonon energy. The solid curves in Fig. 6 are the best fits of the $E_g(T)$ values using Eq. (2) with the fitting parameters shown in Table 1. The determined average phonon energies are in the range of the measured energies of the Raman modes.

Fig. 6 demonstrates a strong decrease of both energy gaps with increasing temperature so at room temperature $E_g(X) = 1.18$ eV. A reduction in the splitting of the valence bands, from 0.28 eV at 10 K to 0.27 eV at 100 K can also be observed.

PL spectra provide information on the mechanisms of radiative recombination and the nature of defects [26]. The low temperature (4.2 K) PL spectrum in Fig. 7, measured with the extended range detector, contains two non-resolved broad bands: A1 at about 0.99 eV with a full width at half maximum (FWHM) of 160 meV and (A2) at 0.84 eV with a FWHM of 140 meV. The relative intensities of the bands vary at

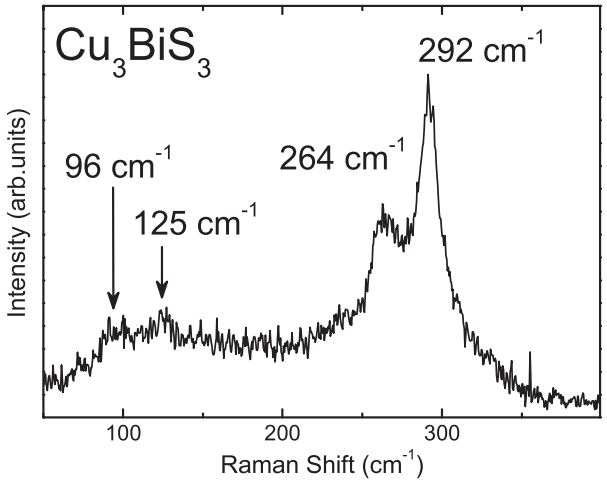

Fig. 4. Raman spectra of the Cu_3BiS_3 thin films.

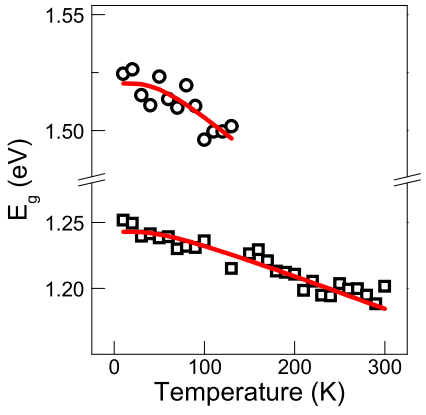

Fig. 6. Temperature dependence of the X and Y bandgap energies E_g; symbols are experimental E_g, and the curves are best fits using Eq. (2).

Table 1
The bandgap E_g, coupling constant S and average phonon energy $<\hbar\omega>$ for the X and Y valence bands, determined by fitting the experimental temperature dependencies of E_g using Eq. (2).

Valence band	E_g (0), eV	S	$<\hbar\omega>$, meV
X	1.24	0.54	6
Y	1.53	0.70	20

different points on the sample, but their spectral positions remain the same.

The dependence of the total integrated PL intensity (I) of both bands on increasing laser power P was fitted to the equation $I \sim P^{\gamma}$. A determined value of $\gamma \approx 0.71$ suggests that these bands are associated with defect related transitions [27]. No significant spectral shifts were observed as the excitation laser power density was increased from 0.26 to 2 W/cm^2.

The PL intensity of the A1 band increases at a greater rate than that of the A2 band, as clearly seen in Fig. 8 which shows spectra excited with laser power densities of 0.26, 0.78 and 2 W/cm^2 and normalised to the A2 band intensity for 2 W/cm^2. The low energy tail of the A2 band is cut-off beyond the 1.7 μm limit of the PMT used for this measurement.

The temperature dependence of the PL spectra from 5 to 90 K is shown in Fig. 9(a). These spectra reveal significant water absorption at 0.9 eV. The spectral positions of the A1 and A2 bands do not shift within this temperature range. Also the A1 band is seen to quench at a greater rate than A2. An Arrhenius plot of the temperature quenching for the integrated intensity of both bands I is shown in Fig. 9(b), revealing a straight line region between 50 and 90 K.

The best fit of the experimental data points in this region was achieved assuming one recombination channel model $I(T) = I_0 [1 + Aexp(-E_a / kT)]$, where I_0 (intensity at the lowest temperature), E_a (activation energy) and A are the fitting parameters and k is the Boltzmann constant. An activation energy of 40 ± 4 meV is determined.

The excitation intensity and temperature analysis of the bands suggests a preliminary interpretation as the recombination of electrons bound to deep donors and holes bound to deep acceptors [28]. According to this model, recombination of electrons and holes of close highly localised donors and acceptors with different spatial separations can generate several peaks each corresponding to a particular separation.

An increase in the laser intensity leads to recombination of closer located donor–acceptor pairs, which have greater Coulomb energy. This redistributes the intensity towards higher energy peaks.

For merged peaks this process results in a spectral shift of the PL band maximum towards higher energy with increasing laser power, whereas redistribution of intensities is a characteristic of non-merged

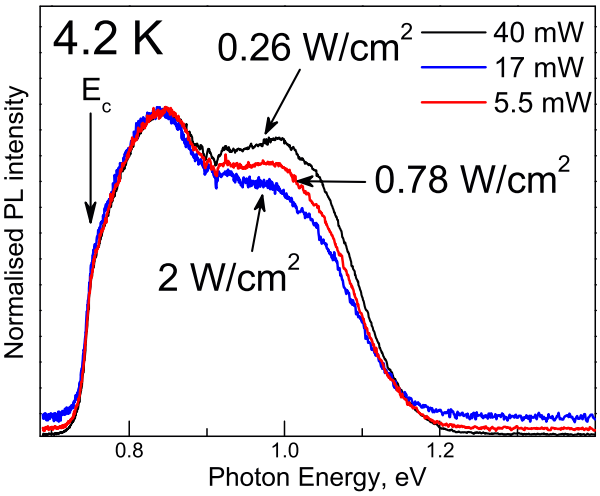

Fig. 8. Normalised PL spectra at different excitation powers (E_c is the detector cut-off energy).

peaks. Ionisation of a shallower defect, located at 40 meV from the valence or conduction band, can cause the observed temperature quenching of both bands. An AQE spectrum, shown in Fig. 10(a), demonstrates a photoresponse of about 1% in the photon range of 1.1–2.3 eV. A similar photoresponse also measured using Eu^{+3} electrolyte has been reported in [9]. Varying the potential with respect to the reference electrode the authors of [9] derived the doping density values. AQE depends on absorption coefficient α as [29],

$$\mathrm{AQE} = 1 - \exp(-\alpha W), \tag{3}$$

where W is the width of the space charge region. For a direct allowed transition, the dependence of the absorption coefficient on the photon energy $h\nu$ should follow the relation,

$$\alpha h\nu \propto \left(h\nu - E_g\right)^{1/2}, \tag{4}$$

Therefore $[h\nu\, ln(1 - AQE)]^2$, as a function of photon energy $h\nu$, should follow a straight line. Fig. 10(b) demonstrates a clear linearity of the $[h\nu\, ln(1 - AQE)]^2$ dependence on $h\nu$ suggesting a direct allowed nature of the bandgap in Cu_3BiS_3. Extending this line to the intersection with the $h\nu$ axis, as shown in Fig. 10(b), gives an estimate of E_g = 1.22 eV which is close to that determined from PR measurements at room temperature.

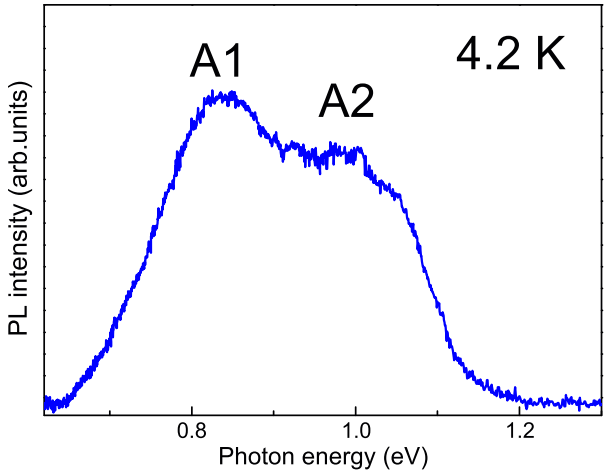

Fig. 7. Extended PL spectrum of Cu_3BiS_3.

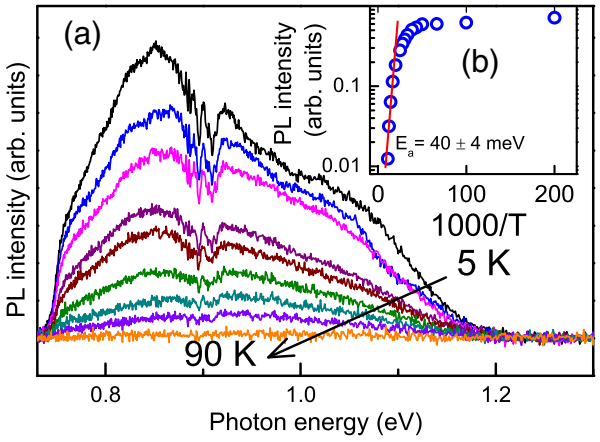

Fig. 9. Temperature dependence of the PL spectra (a), Arrhenius plot of the temperature quenching of the A1 and A2 band integrated intensity (o experimental data, – fitted straight line) (b).

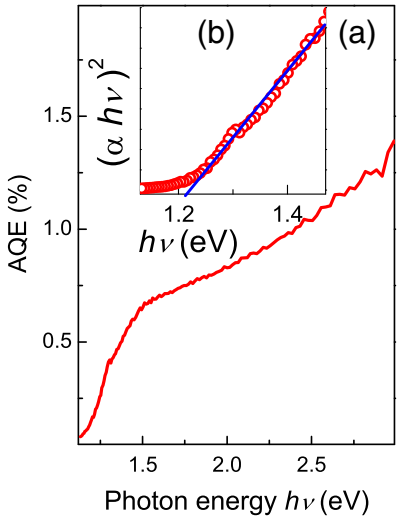

Fig. 10. Apparent quantum efficiency of the Cu_3BiS_3 film (a), the dependence of $[\alpha h\nu]^2$ on $h\nu$ and estimation of E_g (b).

4. Conclusion

Thin films of *p*-type Cu_3BiS_3 with good lateral homogeneity and wittichenite orthorhombic lattice structure have been synthesised by thermal annealing of Cu and Bi precursor, magnetron sputtered on Mo/glass substrate, with a layer of thermo-evaporated S. Photoreflectivity spectra at 10 K reveal two band gaps, at 1.24 and 1.53 eV, which were associated with the X and Y valence sub-bands, respectively, split due to the crystal field influence. Two broad emission bands at 0.99 and 0.84 eV were observed in the PL spectra at low temperatures. Excitation power changes did not shift the bands causing a redistribution of PL intensity towards the higher energy band. Both bands were quenching at a temperature of 90 K. An activation energy of 40 meV was determined by the Arrhenius analysis of the quenching. The photocurrent excitation spectra demonstrate a photoresponse of the films and suggest a direct allowed nature of the band gap.

Acknowledgements

This work was supported by the EPSRC Materials in Engineering (4.5.01), SUPERGEN programme “Photovoltaics for the 21st Century”, KTF, BCFR (F11MC-021), RFBR grants 11-03-00063, 13-03-96032, 12-U3-1006, and 14-02-00080 and Estonian Science Foundation Grant G-8282.

References

[1] M.A. Green, K. Emery, Y. Hishikawa, W. Warta, Solar cell efficiency tables (version 37), Prog. Photovolt. Res. Appl. 19 (2011) 84.
[2] B.A. Andersson, Materials availability for large-scale thin-film photovoltaics, Prog. Photovolt. Res. Appl. 8 (2000) 61.
[3] S. Siebentritt, S. Schorr, Kesterites—a challenging material for solar cells, Prog. Photovoltaics 20 (2012) 512.
[4] F. Luckert, D.I. Hamilton, M.V. Yakushev, N. Beattie, G. Zoppi, M. Moynihan, I. Forbes, A.V. Karotki, A.V. Mudryi, M. Grossberg, J. Krustok, R.W. Martin, Optical properties of high quality $Cu_2ZnSnSe_4$ thin films, Appl. Phys. Lett. 99 (2011) 062104-1.
[5] U.S.Geological survey, Mineral Commodity Summaries, January 2012.
[6] P.K. Nair, L. Huang, M.T.S. Nair, H. Hu, E.A. Meyers, R.A. Zingaro, Formation of p-type Cu_3BiS_3 absorber thin films by annealing chemically deposited Bi_2S_3–CuS thin films, J. Mater. Res. 12 (1997) 651.
[7] V. Estrella, M.T.S. Nair, P.K. Nair, Semiconducting Cu_3BiS_3 thin films formed by the solid-state reaction of CuS and bismuth thin films, Semicond. Sci. Technol. 18 (2003) 190.
[8] F. Mesa, G. Gordillo, Effect of preparation conditions on the properties of Cu_3BiS_3 thin films grown by a two-step process, J. Phys. Conf. Ser. 167 (012019) (2009) 1.
[9] D. Colombara, L.M. Peter, K. Hutchings, K.D. Rogers, S. Schäfer, J.T.R. Dufton, M.S. Islam, Formation of Cu_3BiS_3 thin films via sulfurization of Bi–Cu metal precursors, Thin Solid Films 520 (2012) 5165.
[10] M. Kumar, C. Persson, Cu_3BiS_3 as a potential photovoltaic absorber with high optical efficiency, Appl. Phys. Lett. 102 (2013) 062109-1.
[11] F. Mesa, G. Gordillo, Th. Dittrich, K. Ellmer, R. Baier, S. Sadewasser, Transient surface photovoltage of p-type Cu_3BiS_3, Appl. Phys. Lett. 96 (2010) 082113-1.
[12] C. Tablero, Photovoltaic application of O-doped Wittichenite–Cu_3BiS_3: from microscopic properties to maximum efficiencies, Prog. Photovolt. Res. Appl. 21 (2013) 894.
[13] J. Krustok, H. Collan, M. Yakushev, K. Hjelt, The role of spatial potential fluctuations in the shape of the PL bands of multinary semiconductor compounds, Phys. Scr. T79 (1999) 179.
[14] I. Dirnstorfer, Mt. Hofmann, M.D. Lampert, F. Karg, B.K. Meyer, CuIn(Ga)Se_2 solar cells: characterization of the absorber material, Inst. Phys. Conf. Ser. 152 (1998) 233.
[15] F.H. Pollak, H. Shen, Modulation spectroscopy of semiconductors: bulk/thin film, microstructures, surfaces/interfaces and devices, Mater. Sci. Eng. R10 (1993) 275.
[16] D. Colombara, L.M. Peter, K.D. Rogers, K. Hutchings, Thermochemical and kinetic aspects of the sulfurization of Cu–Sb and Cu–Bi thin films, J. Solid State Chem. 186 (2012) 36.
[17] B.M. Basol, V.K. Kapur, Deposition of $CuInSe_2$ films by a two-stage process utilizing E-beam evaporation, IEEE Trans. Electron Devices 37 (1990) 418.
[18] I. Forbes, K. Reddy, D. Johnston, R.W. Miles, D.W. Lane, K.D. Rogers, A. Chapman, R.f. sputtering of high-quality Cu/In precursor layers and conversion to $CuInS_2$ using elemental sulfidization processes, J. Mater. Sci. Mater. Electron. 14 (2003) 567.
[19] P. Maiello, G. Zoppi, R.W. Miles, N. Pearsall, I. Forbes, Chalcogenisation of Cu–Sb metallic precursors into Cu3Sb(SexS1 − x)3, Sol. Energy Mater. Sol. Cells 113 (2013) 186.
[20] D.E. Aspnes, in: M. Balkanski (Ed.), Handbook on Semiconductors II, vol. 2, North-Holland, Amsterdam, 1980, p. 109, (Chap. 4A).
[21] T. Raadik, J. Krustok, M.V. Yakushev, Photoreflectance study of AgGaTe2 single crystals, Phys. B Condens. Matter 406 (2011) 418.
[22] M.V. Yakushev, F. Luckert, C. Faugeras, A.V. Karotki, A.V. Mudryi, R.W. Martin, Diamagnetic shift of the A free exciton in CuGaSe2, Appl. Phys. Lett. 97 (2010) 152110-1.
[23] J.L. Shay, J.H. Wernick, Ternary Chalcopyrite Semiconductors-Growth, Electronic Properties, and Applications, Pergamon Press, Oxford, 1975.
[24] J.L. Shay, B. Tell, L.M. Schiavone, H.M. Kasper, F. Thiel, Energy bands of $AgInS_2$ in the chalcopyrite and orthorhombic structures, Phys. Rev. B 9 (1974) 1719.
[25] K.P. O'Donnell, X. Chen, Temperature dependence of semiconductor band gaps, Appl. Phys. Lett. 58 (1991) 2924.
[26] H.B. Bebb, E.W. Williams, in: R.K. Willardson, A.C. Beer (Eds.), Semiconductors and Semimetals, Academic, New York, 1972.
[27] T. Schmidt, K. Lischka, W. Zulehner, Excitation-power dependence of the near-band-edge photoluminescence of semiconductors, Phys. Rev. B 45 (1992) 8989.
[28] J. Krustok, J. Raudoja, M. Krunks, H. Mandar, H. Collan, Nature of the native deep localized defect recombination centers in the chalcopyrite and orthorhombic $AgInS_2$, J. Appl. Phys. 88 (2000) 205.
[29] J. Scragg, P.J. Dale, L.M. Peter, G. Zoppi, I. Forbes, New routes to sustainable photovoltaics: evaluation of Cu_2ZnSnS_4 as an alternative absorber material, Phys. Stat. Sol. (b) 245 (2008) 1772.